Composition and yields of secondary organic aerosol formed from OH radical-initiated reactions of linear alkenes in the presence of NO x : Modeling and measurements

ARTICLE *in* ATMOSPHERIC ENVIRONMENT · FEBRUARY 2009

Impact Factor: 3.28 · DOI: 10.1016/j.atmosenv.2008.12.004

4 AUTHORS, INCLUDING:

Yong Bin Lim
Korea Institute of Science and Technology
27 PUBLICATIONS **1,047** CITATIONS

SEE PROFILE

Atmospheric Environment 43 (2009) 1349–1357

Contents lists available at ScienceDirect

Atmospheric Environment

journal homepage: www.elsevier.com/locate/atmosenv

Composition and yields of secondary organic aerosol formed from OH radical-initiated reactions of linear alkenes in the presence of NO_x: Modeling and measurements

Aiko Matsunaga [1], Kenneth S. Docherty [2], Yong B. Lim [3], Paul J. Ziemann*,[4]

Air Pollution Research Center, University of California, Riverside, CA 92521, USA

ARTICLE INFO

Article history:
Received 1 September 2008
Received in revised form
2 December 2008
Accepted 3 December 2008

Keywords:
Secondary organic aerosol
OH radical
Modeling
Particle-phase chemistry
Reaction mechanism
Hydrocarbon oxidation
Oligomers

ABSTRACT

The products and mechanism of secondary organic aerosol (SOA) formation from the OH radical-initiated reactions of linear alkenes in the presence of NO_x were investigated in an environmental chamber. The SOA consisted primarily of products formed through reactions initiated by OH radical addition to the C=C double bond, including β-hydroxynitrates and dihydroxynitrates, as well as cyclic hemiacetals, dihydrofurans, and dimers formed from particle-phase reactions of dihydroxycarbonyls. 1,4-Hydroxynitrates formed through reactions initiated by H-atom abstraction also appeared to contribute. Product yields and OH radical and alkoxy radical rate constants taken from the literature or calculated using structure–reactivity methods were used to develop a quantitative chemical mechanism for these reactions. SOA yields were then calculated using this mechanism with gas-particle partitioning theory and estimated product vapor pressures for comparison with measured values. Calculated and measured SOA yields agreed very well at high carbon numbers when semi-volatile products were primarily in the particle phase, but diverged with decreasing carbon number to a degree that depended on the model treatment of dihydroxycarbonyls, which appeared to undergo reversible reactions in the particle phase. The results indicate that the chemical mechanism developed here provides an accurate representation of the gas-phase chemistry, but the utility of the SOA model depends on the partitioning regime. The results also demonstrate some of the advantages of studying simple aerosol-forming reactions in which the majority of products can be identified and quantified, in this case leading to insights into both gas- and particle-phase chemistry.

1. Introduction

One purpose of experimental studies of aerosols is to provide data for developing detailed models of the physical and chemical processes controlling atmospheric aerosol properties such as chemical composition, size distribution, light scattering and absorption, hygroscopicity, and cloud condensation nucleating activity. These models in turn are incorporated in simplified form into local, regional, and global scale models, which can be used to understand collective effects and to develop strategies for minimizing the impacts of human activities on air quality, visibility, climate, and human and ecosystem health (Seinfeld and Pandis, 1998). A major challenge is the development of models of secondary organic aerosol (SOA) formation, a complex process in which gas- and particle-phase reactions involving organic compounds and oxidants lead to an array of products that can partition to particles (Kroll and Seinfeld, 2008). In most models, these processes are treated using simple empirical parameterizations (Kanakidou et al., 2005). In a few cases, however, detailed mechanisms of gas-phase chemical reactions have been combined with gas-particle partitioning, emissions, and meteorology to predict the chemical composition and mass of atmospheric SOA (Johnson et al., 2006). Unfortunately, current models tend to underpredict atmospheric SOA mass concentrations (de Gouw et al., 2005; Heald et al., 2005; Johnson et al., 2006; Volkamer et al., 2006) probably for a variety of reasons. For example, discrepancies have been attributed to problems with laboratory SOA yield

* Corresponding author. Tel.: +1 951 827 5127; fax: +1 951 827 5004.
E-mail address: paul.ziemann@ucr.edu (P.J. Ziemann).
[1] Also in Department of Chemistry.
[2] Also in Environmental Toxicology Graduate Program. Present address: Department of Chemistry and Biochemistry, and Cooperative Institute for Research in the Environmental Sciences (CIRES), University of Colorado, Boulder, CO, USA.
[3] Also in Department of Chemistry. Present address: Department of Environmental Sciences, Rutgers University, New Brunswick, NJ, USA.
[4] Also in the Department of Environmental Sciences, Department of Chemistry, and Environmental Toxicology Graduate Program.

1352-2310/$ – see front matter © 2008 Elsevier Ltd. All rights reserved.
doi:10.1016/j.atmosenv.2008.12.004

measurements (Presto and Donahue, 2006; Kroll et al., 2007), and to an absence in models of possible sources of SOA such as heterogeneous chemistry (Johnson et al., 2006), first-generation products of anthropogenic VOC oxidation (Volkamer et al., 2006), semi-volatile emissions (Robinson et al., 2007), higher-generation reaction products (Donahue et al., 2006), and cloud processing (Altieri et al., 2006).

In general, models predict that global SOA is derived primarily from the oxidation of biogenic alkenes, in particular linear, branched, and cyclic terpenes consisting of isoprene (C_5H_8), monoterpenes ($C_{10}H_{16}$), and sesquiterpenes ($C_{15}H_{24}$) (Kanakidou et al., 2005). Recent field studies (Weber et al., 2007) also indicate that terpene oxidation is responsible for a large fraction of SOA in urban areas. In spite of the importance of these reactions and the considerable effort expended investigating gas- and particle-phase products, the chemical mechanisms are poorly understood (Atkinson and Arey, 2003; Kroll and Seinfeld, 2008). Recently, we investigated SOA products formed from OH radical-initiated reactions of simple linear alkenes in the presence of NO_x, conditions representative of a polluted atmosphere. Such studies provide insights into products and mechanisms of more complex alkene reactions. Major β-hydroxynitrate and dihydroxynitrate SOA products were identified and quantified and used to determine some of the branching ratios for reaction pathways leading to their formation (Matsunaga and Ziemann, in press). Here, those results were used with additional SOA composition information obtained in that study but not previously reported, along with product data from the literature and structure–reactivity calculations of rate constants to develop a quantitative chemical mechanism for reactions of linear 1-alkenes and internal alkenes. This mechanism was then used to model the formation of SOA and the results were compared with measured SOA yields.

2. Experimental

2.1. Chemicals

The C_8–C_{17} linear 1-alkenes, 7-tetradecene, 7-pentadecene, 8-heptadecene, dioctyl sebacate, and NO were obtained from commercial suppliers (Matsunaga and Ziemann, in press). Methyl nitrite was synthesized (Taylor et al., 1980) and stored in liquid nitrogen until used, and O_3 was generated using a Welsbach T-408 O_3 generator.

2.2. Environmental chamber method

Alkenes were reacted with OH radicals in the presence of NO_x in a 5900 L PTFE environmental chamber filled with clean, dry air (<5 ppbv hydrocarbons, <1% RH) at ~25 °C and atmospheric pressure. The reaction mixture was ~200–400 μg m^{-3} of dioctyl sebacate (DOS) seed particles added from an evaporation–condensation source and 1 (0.5 and 0.3 for 1- and 8-heptadecene), 5, and 5 ppmv of alkene, methyl nitrite, and NO. Reactions were initiated by turning on blacklights to form OH radicals by methyl nitrite photolysis (Atkinson et al., 1981). The average OH radical concentration for 6 min of reaction was ~3×10^7 cm^{-3}, determined from 40 to 50% of alkene that reacted and reaction rate constants (Aschmann and Atkinson, 2008).

2.3. Particle and gas analysis

A thermal desorption particle beam mass spectrometer (TDPBMS) was used to analyze particle composition in real-time (Tobias et al., 2000) and by temperature-programmed thermal desorption (TPTD) (Tobias and Ziemann, 1999). Air was sampled into the TDPBMS and particles were formed into a beam and impacted on a polymer-coated metal vaporizer (Chattopadhyay and Ziemann, 2005). For real-time analysis, the vaporizer was resistively heated to 160 °C and particles evaporated on impact. Vapor was ionized by 70 eV electrons and analyzed in a quadrupole mass spectrometer. For TPTD analysis, the vaporizer was cooled to −40 °C, particles were collected for 30 min, and the vaporizer was allowed to warm to −5 °C and then heated to 200 °C using a 2 °C min^{-1} ramp to desorb and separate compounds by volatility prior to mass analysis.

SOA mass concentration, M_{SOA}, was calculated as the difference in aerosol volume concentrations of seed and SOA + seed measured using a scanning mobility particle sizer (SMPS) (Wang and Flagan, 1990), multiplied by an SOA density of 1.13 g cm^{-3} measured using a microliter syringe, a balance, and a dried filter extract of liquid SOA formed in the reaction of 1-tetradecene. Alkenes were collected on Tenax TA solid adsorbent before and after reaction and analyzed by GC-FID (Docherty et al., 2005) to determine the mass of alkene reacted, ΔM_{alkene}. SOA yields were calculated as $Y_{SOA} = M_{SOA}/\Delta M_{alkene}$ (Odum et al., 1996).

3. Development of a chemical mechanism and model of SOA formation

3.1. Reaction mechanism

The mechanism of OH radical-initiated reactions of linear alkenes in the presence of NO_x is shown in Fig. 1, where R_1 represents an alkyl group and R_2 represents an H-atom in 1-alkenes and an alkyl group in internal alkenes. Detailed discussions of the pathways leading to products **P1**–**P10** can be found in Atkinson and Arey (2003). The reaction is initiated primarily by addition of an OH radical to the C=C double bond, although H-atom abstraction is significant. Addition forms two β-hydroxyalkyl radical isomers, which react with O_2 to form β-hydroxyperoxy radicals that react with NO, forming β-hydroxynitrates [**P1**, **P2**] or β-hydroxyalkoxy radicals. The β-hydroxyalkoxy radicals can react with O_2, decompose, or isomerize. Reaction with O_2 forms α-hydroxycarbonyls [**P3**, **P4**], but is not important for the large alkenes of interest here (Atkinson, 2007). Decomposition followed by reaction with O_2 forms two aldehydes [**P5**, **P6**] (and a small fraction of other products that are not shown, such as 1,4-hydroxycarbonyls and 1,4-hydroxynitrates; Aschmann and Atkinson, in preparation), and isomerization followed by reaction with O_2 forms dihydroxyperoxy radicals that react similarly to β-hydroxyperoxy radicals. The products are dihydroxynitrates [**P7**, **P8**] and dihydroxyalkoxy radicals that isomerize and react with O_2 to form dihydroxycarbonyls [**P9**, **P10**]. Dihydroxycarbonyls [**P9**, **P10**] can isomerize to cyclic hemiacetals [**P11**] that can dehydrate to dihydrofurans [**P12**], or they can form dimers [**P13**–**P15**]. On the basis of other studies (Holt et al., 2005; Gong et al., 2005; Lim and Ziemann, 2005; Kern and Spiteller, 1996) and results presented below, dihydroxyketones [**P9**] probably form mostly cyclic hemiacetals [**P11**] and dihydrofurans [**P12**], whereas dihydroxyaldehydes [**P10**] form mostly dimers [**P13**–**P15**].

3.2. Branching ratios and product yields

The branching ratios shown in Fig. 1 are defined as $\alpha_i = r_i/\sum r_i$, where r_i is the rate a species reacts by pathway i and the sum is over all pathways by which the species reacts. The sum of branching ratios for a species is 1. Note that α_4, α_6, α_8, α_{10}, α_{12}, α_{14}, and α_{16} are associated with the portion of the mechanism labeled "same pathways" and correspond to α_3, α_5, α_7, α_9, α_{11}, α_{13}, and α_{15}, respectively. Values used in the model are given in Table 1, and

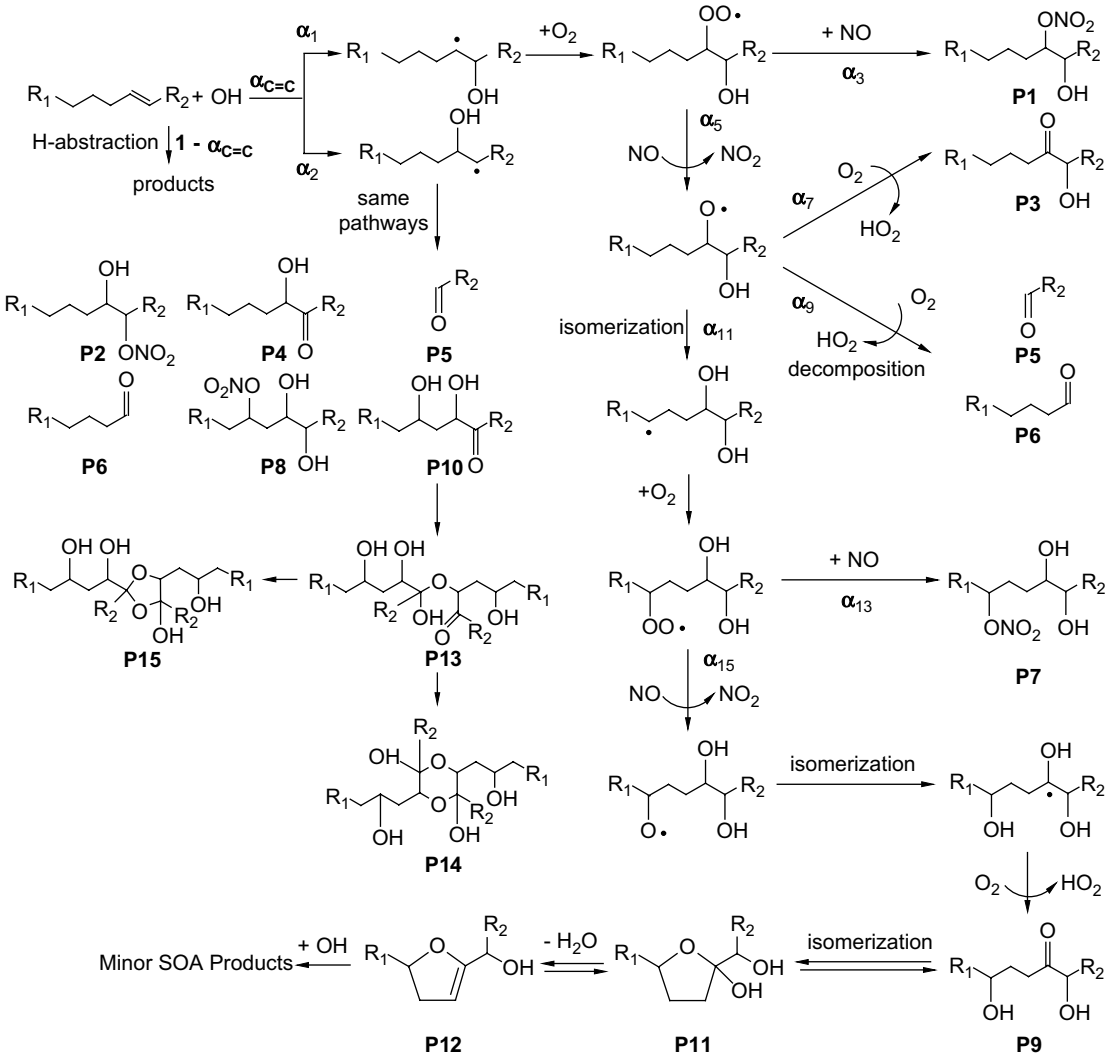

Fig. 1. Mechanism of the OH radical-initiated reaction of linear alkenes in the presence of NO_x. R_1 represents an alkyl group and R_2 represents an H-atom in 1-alkenes and an alkyl group in internal alkenes.

the methods by which they were calculated are described in Supplementary Information. The values are consistent with experimental data (Matsunaga and Ziemann, in press; Aschmann and Atkinson, in preparation) and with rate constants for OH radical (Kwok and Atkinson, 1995; Aschmann and Atkinson, 2008; Nishino et al., in press) and alkoxy radical reactions (Atkinson, 2007). Molar yields normalized for OH radical addition [(moles of product/moles of alkene reacted)/$\alpha_{C=C}$], which are equal to the product of the branching ratios along the pathway leading to the reaction product divided by $\alpha_{C=C}$, were calculated using branching ratios in Table 1 and are given in Table 2 along with molar yields of 1,4-hydroxynitrates normalized for H-atom abstraction [(moles of product/moles of alkene reacted)/(1 − $\alpha_{C=C}$)].

Table 1
Branching ratios used for modeling SOA formation from OH radical-initiated reactions of linear alkenes in dry air in the presence of NO_x.

Branching ratio	1-Alkenes	Internal alkenes
$\alpha_{C=C}$[a]	$\alpha_{C=C}$	$\alpha_{C=C}$
α_1	0.70 × $\alpha_{C=C}$	0.50 × $\alpha_{C=C}$
α_2	0.30 × $\alpha_{C=C}$	0.50 × $\alpha_{C=C}$
α_3, α_4	0.14	0.15
α_5, α_6	0.86	0.85
α_7, α_8	0.00	0.00
α_9	0.51	0.67
α_{10}	0.34	0.67
α_{11}	0.49	0.33
α_{12}	0.66	0.33
α_{13}, α_{14}	0.08	0.02
α_{15}, α_{16}	0.92	0.98

[a] $\alpha_{C=C} = k_{add}/(k_{add} + k_{abs})$. For 1-alkenes, $k_{abs} = 2.47 + 1.4 \times (CN\text{-}5)$ and $k_{add} = 28 + 9 \times [1 - \exp(-0.35 \times (CN\text{-}3))]$. For *cis* and *trans* internal alkenes, $k_{abs} = 4.93 + 1.4 \times (CN\text{-}8)$, $k_{add}(cis) = 56.4$, and $k_{add}(trans) = 64$. CN is the alkene carbon number. See Supplementary Information for additional details.

3.3. H-atom abstraction and secondary reactions

First-generation products formed through H-atom abstraction pathways and second-generation products formed through reactions of first-generation products with OH radicals have the potential to form SOA, but the reaction mechanisms are complex and the product contributions are difficult to quantify (Lim and Ziemann, 2005). For simplicity, in a first set of calculations it was assumed that the only contribution of H-atom abstraction pathways to SOA formation was from 1,4-hydroxynitrates, and that the formation of SOA products from secondary reactions with OH radicals was negligible. The 1,4-hydroxynitrates were assumed to

Table 2
Normalized molar yields of products used to model SOA formation from OH radical addition and H-atom abstraction reactions of linear alkenes in dry air in the presence of NO_x.

Product	Normalized molar yield[a]	
	1-Alkenes	Internal alkenes
OH radical addition		
β-Hydroxynitrates		
P1	0.098	0.075
P2	0.042	0.075
P1 + P2	0.140	0.150
β-Hydroxycarbonyls		
P3	0.000	0.000
P4	0.000	0.000
Carbonyls		
P5	0.395	0.570
P6	0.395	0.570
P5 + P6		1.140
Dihydroxynitrates		
P7	0.024	0.003
P8	0.014	0.003
P7 + P8	0.038	0.006
Dihydroxycarbonyls		
P9	0.271	0.137
P10	0.157	0.137
P9 + P10	0.428	0.274
H-atom abstraction		
1,4-Hydroxynitrates	0.1	0.1

[a] Normalized molar yield (OH radical addition) = (moles of product/moles of alkene reacted)/$\alpha_{C=C}$. Normalized molar yield (H-atom abstraction) = (moles of product/moles of alkene reacted)/(1 − $\alpha_{C=C}$). Values of $\alpha_{C=C}$ calculated using equations in Table 1.

be formed with an H-atom abstraction-normalized molar yield of 0.1 estimated from measured yields (Lim and Ziemann, 2005; Reisen et al., 2005) and consistent with values recently determined by us for C_{13}–C_{17} *n*-alkanes. The major first-generation products of H-atom abstraction should be alkyl nitrates, 1,4-hydroxycarbonyls, and 1,4-hydroxynitrates, as observed in similar reactions of *n*-alkanes (Lim and Ziemann, 2005; Reisen et al., 2005). As shown below, thermal desorption profiles showed no alkyl nitrates or 1,4-hydroxycarbonyls, which would be easily detected since they would desorb before β-hydroxynitrates. Most likely, alkyl nitrates were too volatile to form SOA, and 1,4-hydroxycarbonyls were absent because they isomerized to cyclic hemiacetals that dehydrated to volatile dihydrofurans (more volatile than **P12** in Fig. 1 because they do not have the hydroxy group) (Holt et al., 2005; Lim and Ziemann, 2005). Dihydrofurans may have then reacted with OH radicals, but would mostly form volatile carbonylesters (Martin et al., 2002).

In a second set of calculations, upper limits to the possible contributions of secondary reaction products to SOA yields were estimated using a kinetic model written in FACSIMILE that included gas-phase reactions and gas–particle partitioning. The rate constants for H-atom abstraction and OH radical addition reactions for alkenes were calculated using equations obtained from Kwok and Atkinson (1995) and Nishino et al. (in press) given in Supplementary Information, and rate constants for H-atom abstraction from saturated products were calculated using the structure–reactivity method of Kwok and Atkinson (1995). An equation for the time-dependent OH radical concentration was obtained from multiple measurements of alkene concentrations made during an experiment with 1-decene. Gas–particle partitioning was calculated as described below using measured aerosol mass concentrations. Yields of products formed from alkenes by H-atom abstraction followed by OH radical addition were calculated by assuming all H-atom abstraction products (unsaturated alkyl nitrates, 1,4-hydroxycarbonyls, and 1,4-hydroxynitrates) stayed in the gas phase during the entire reaction, thereby overestimating the formation of secondary reaction products. Yields of products formed from alkenes by OH radical addition followed by H-atom abstraction were calculated by assuming that during the reaction all OH-addition products (saturated β-hydroxynitrates, dihydroxynitrates, and dihydroxycarbonyls) other than carbonyls underwent gas–particle partitioning to the same extent as β-hydroxynitrates, and that in the particle phase they did not react with OH radicals. Since the actual vapor pressures of these compounds are the same or less than β-hydroxynitrates, these calculations also overestimate the formation of secondary reaction products. Because carbonyls are volatile fragmentation products and generally react with OH radicals to form even smaller carbonyls (Atkinson and Arey, 2003), it was assumed that their reactions did not to contribute to SOA formation. Calculated molar yields of products were converted to mass yields using ratios of the molecular weights of product and alkene, and these mass yields were then used as upper limit estimates of the contribution of these reactions to the SOA yields.

3.4. Gas–particle partitioning

The equilibrium gas–particle partitioning of products was calculated using the theory of Pankow (1994), which assumes that particulate organic matter (POM) is a single, liquid organic phase. This assumption seems valid since dried filter extracts were clear liquids and when seed particle concentrations were increased from ~200 to ~1000 μg m^{-3} in 7-tetradecene experiments the SOA yield of β-hydroxynitrates was ~4 times larger, indicating enhanced gas-to-particle partitioning. Partitioning coefficients were calculated from compound vapor pressures, activity coefficients, and mean molecular weights of POM and used with organic aerosol mass concentration, M_O (M_{SOA} + M_{seed}), to calculate the fraction of each compound in the particle phase. Activity coefficients were assumed to be unity (Seinfeld et al., 2001) and the mean molecular weight of POM was assumed to be that of β-hydroxynitrates. Product vapor pressures were estimated from measured partitioning of β-hydroxynitrates and group contribution calculations described in Fig. S1 and Table S1.

3.5. SOA yield calculations

For each alkene, the total (gas + particle) mass concentration of each product was calculated by multiplying the normalized molar yield in Table 2 by $\alpha_{C=C}$ for OH radical addition and 1 − $\alpha_{C=C}$ for H-atom abstraction, the ratio of the molecular weights of product and alkene, and ΔM_{alkene}. Product mass concentrations, partitioning coefficients, and seed particle mass concentration were then used to calculate the contributions of each product to the SOA yield (Colville and Griffin, 2004). In one case, it was assumed that dihydroxycarbonyls [**P9**, **P10**] existed entirely in the particle phase as non-volatile cyclic hemiacetals [**P11**], dihydrofurans [**P12**], and dimers [**P13**–**P15**] rather than in gas–particle partitioning equilibrium.

4. Results and discussion

4.1. Measured SOA products

Thermal desorption profiles and real-time mass spectra of SOA formed from reactions of 1-tetradecene and 7-tetradecene are shown in Fig. 2. In Fig. 2A, total ion (TI) signal is proportional to organic mass (Crable and Coggeshall, 1958), so profiles represent distributions of SOA mass with respect to volatility. For both

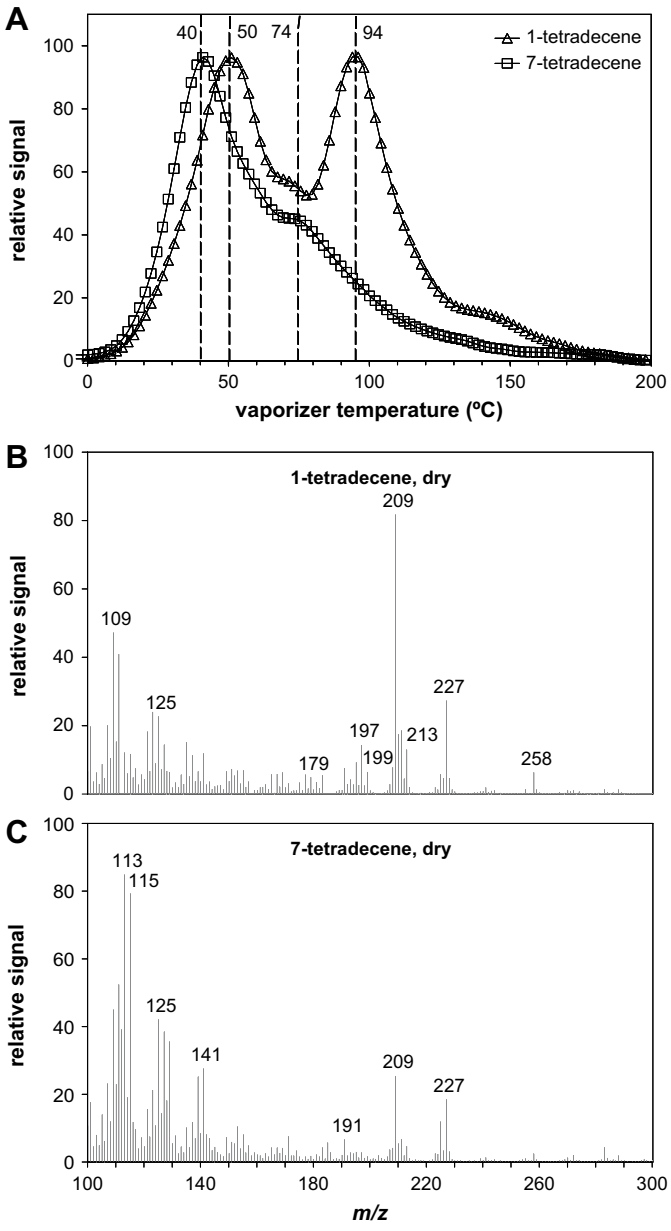

Fig. 2. (A) Total ion (m/z 50–500) thermal desorption profiles and (B, C) real-time mass spectra of SOA formed from the OH radical-initiated reactions of 1-tetradecene and 7-tetradecene in dry air in the presence of NO_x. In Fig. 2A, signals from DOS seed particles were removed by multiplying the m/z 185 profiles (due overwhelmingly to DOS) by the ratio of (total ion)/(m/z 185) signals measured for DOS seed particles in real-time, and then subtracting. Thermal desorption profiles were smoothed and normalized to peak values.

reactions, there are peaks at 40–50 °C and 70–80 °C. For 1-tetradecene, a large peak is also observed at 90–100 °C, whereas for 7-tetradecene only a tail appears in this temperature range. The first two peaks are from β-hydroxynitrates [**P1**, **P2**] and dihydroxynitrates [**P7**, **P8**]; their mass spectra after HPLC separation, desorption profiles of characteristic ions, fragmentation pathways, and yields are discussed elsewhere (Matsunaga and Ziemann, in press). Those formed from reactions of 1-tetradecene and 7-tetradecene have characteristic peaks at m/z 179, 197, and 199, and at m/z 97 and 115, respectively.

Peaks at m/z 227 and 209 in Fig. 2B, C are characteristic of cyclic hemiacetals [**P11**] and dihydrofurans [**P12**], the ions being formed by loss of OH from the molecular ion (Gong et al., 2005; Lim and Ziemann, 2005). These compounds have low vapor pressures, as indicated by thermal desorption profiles shown in Fig. 3A. The cyclic hemiacetal desorbed after the dihydrofuran because the extra hydroxy group lowers its vapor pressure. These profiles overlap with a large peak at 90–100 °C in the TI profile in Fig. 2A, indicating the compounds may contribute significant SOA mass. This product assignment is supported by results shown in Fig. 3B. In this experiment, 20 ppmv of O_3 was added to the chamber 4 h after the lights were turned off. SOA m/z 209 signal disappeared immediately due to reaction of the dihydrofuran double bond with O_3. The m/z 227 signal decayed with a lifetime of ~5–10 min, consistent with measured rates of dehydration of cyclic hemiacetals (Holt et al., 2005). The slower decay of m/z 185 signal, mostly from DOS seed particles, is consistent with H-atom abstraction by NO_3 radicals (Docherty and Ziemann, 2006) formed from reaction of O_3 with NO_2.

The m/z 300–500 region of the real-time mass spectrum from the reaction of 1-tetradecene is shown in Fig. 3C. These peaks extend beyond masses of potential products of secondary reactions with OH radicals. For example, addition of three hydroxy groups and two nitrooxy groups gives a product with molecular weight 368. Instead, these peaks are probably associated with oligomeric species formed by particle-phase reactions. Trends observed in mass spectra for reactions of 1-undecene, 1-dodecene, and 1-tridecene (Fig. 4), and 1-tetradecene (Fig. 3C) support this idea. The mass spectra exhibit two patterns. Peaks at m/z 316, 330, 344, and 358 for the reaction of 1-undecene are shifted by m/z 14, 28, and 42 in mass spectra from reactions of 1-dodecene, 1-tridecene, and 1-tetradecene. This is expected for products of reactions of a homologous series of compounds with successive molecular weights increasing by 14 units. A different pattern is observed at higher masses, however. Peaks at m/z 370, 386, and 402 for the reaction of 1-undecene are shifted by m/z 28, 56, and 84 in mass spectra from reactions of 1-dodecene, 1-tridecene, and 1-tetradecene. This pattern is consistent with the formation of dimers [**P13**–**P15**], where an increase of 14 units in monomer mass increases dimer mass by 28 units.

For these reactions, the most likely monomers are dihydroxyaldehydes [**P10**]. These compounds are major gas-phase products from reactions of C_4–C_8 1-alkenes (Kwok et al., 1996), and synthetic organic chemistry studies showed α-hydroxyaldehydes such as these are unstable and rapidly form dimers (Kern and Spiteller, 1996). Dimers formed from products of the reaction of 1-tetradecene would have molecular weight 488. Peaks at m/z 454, 470, and 486 would correspond to $(M-34)^+$, $(M-18)^+$, and $(M-2)^+$ ions formed by loss of H_2O_2, H_2O, and H_2 from a dimer (or dimer isomers) of mass M, which is reasonable. Desorption profiles of these ions have peaks at 92, 102, and 112 °C, as shown in Fig. 3D, indicating three dimers with different volatilities. If all are dihydroxyaldehyde dimers, then three possible isomer structures are shown in Fig. 1. Product **P13** is a linear hemiacetal and products **P14** and **P15** are cyclic hemiacetals. The latter two structures were proposed for dimers formed from synthesized α-hydroxyaldehydes (Kern and Spiteller, 1996). In the experiment described above in which O_3 was added to the chamber 4 h after the lights were off, m/z 470 and 486 signals decayed in a few minutes (the m/z 454 initial signal was too small to monitor). This indicated the compounds are saturated but can dehydrate to dihydrofurans, as expected for products **P14** and **P15**. Because desorption profiles of dimer ions overlap with the large peak at 90–100 °C in the TI profile in Fig. 2A, these compounds may contribute significant SOA mass. Mass spectra showed no evidence for dimer formation from reactions of internal alkenes, probably because the dihydroxycarbonyl products are dihydroxyketones, which have less of a tendency than dihydroxyaldehydes to form hemiacetals and cyclic dimers.

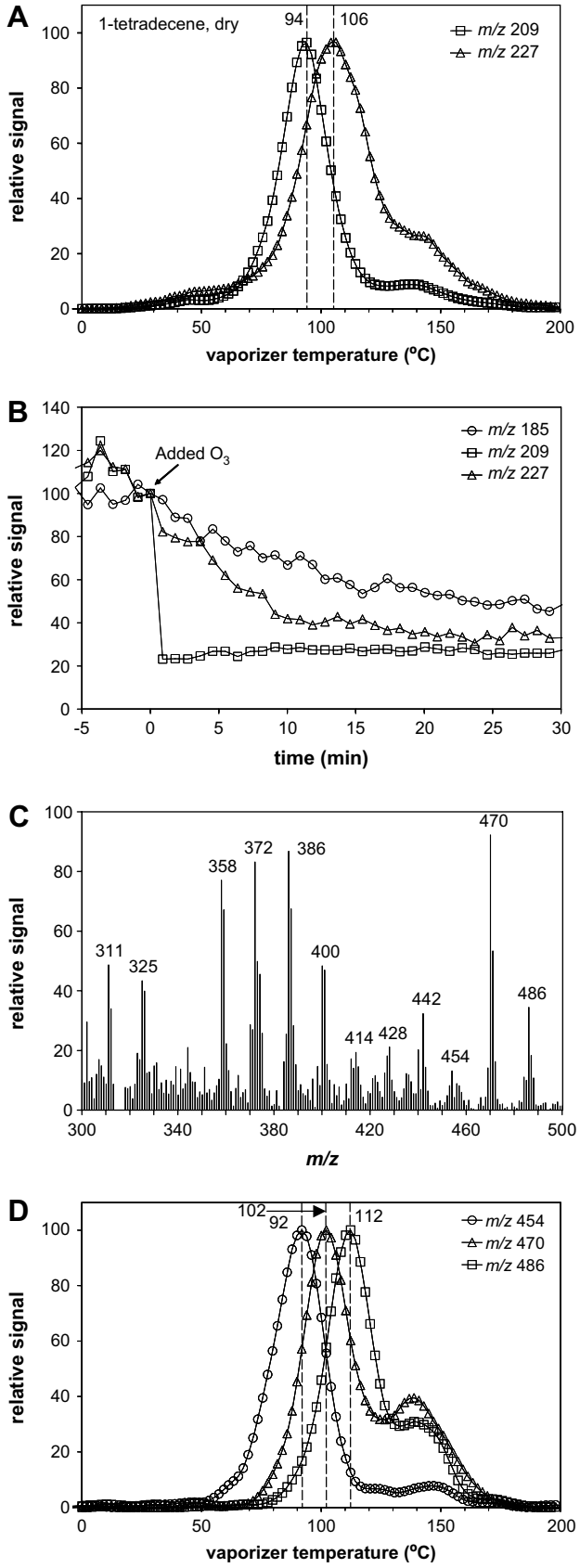

Fig. 3. Mass spectral analyses of SOA formed from OH radical-initiated reactions of 1-tetradecene in dry air in the presence of NO_x. (A) Thermal desorption profiles of ions characteristic of cyclic hemiacetals (m/z 227) and dihydrofurans (m/z 209), (B) real-time signals of these ions after adding O_3 to the chamber containing SOA, (C) real-time mass spectra for m/z 300–500, and (D) thermal desorption profiles of ions characteristic of dimers. A, C, and D were obtained without added O_3. Thermal desorption profiles were smoothed and normalized to peak values, and signals in B were normalized to values at 0 min.

4.2. SOA composition and yields: model results and measurements

Yields of SOA products calculated using the model described above, without estimates of contributions from secondary reaction products, are shown in Fig. 5 and Tables S3 and S4. The difference between Fig. 5A and B and the two halves of Fig. 5C is the model treatment of dihydroxycarbonyls. For results labeled DHC-gpp it was assumed that dihydroxycarbonyls are in gas–particle partitioning equilibrium, whereas for results labeled DHC-nv it was assumed they form non-volatile cyclic hemiacetals, dihydrofurans, and dimers that are entirely in the particle phase. For 1-alkenes $\geq C_{15}$, differences in composition calculated with the two models are small because in both cases dihydroxycarbonyls are almost entirely in the particle phase. Calculated yields of individual products in SOA averaged over this carbon number range were 0.337 (DHC-gpp) and 0.350 (DHC-nv) for dihydroxycarbonyls, 0.121 for β-hydroxynitrates, 0.036 for dihydroxynitrates, and 0.037 for 1,4-hydroxynitrates. The average total yields for SOA products of 0.530 (DHC-gpp) and 0.544 (DHC-nv) agree very well with the average measured SOA yield of 0.518. Note that the measured SOA yields were not used in the development of the model, so this is a comparison of the model output with independent measurements. Dihydroxycarbonyls were calculated to contribute ~65% of SOA mass, consistent with the total ion profile shown in Fig. 2A for the 1-tetradecene reaction where roughly half of the area is contributed by the peak at 94 °C. As the carbon number decreased from C_{15} to C_8, SOA composition changed due to gas–particle partitioning, with compounds being preferentially lost to the gas phase in the order of vapor pressures: 1,4-hydroxynitrates > β-hydroxynitrates ~ dihydroxycarbonyls (DHC-gpp) > dihydroxynitrates > dihydroxycarbonyls (DHC-nv). The differences in composition predicted by the two models also increased dramatically because dihydroxycarbonyls had the largest total (gas + particle) yields of all potential SOA-forming products and, depending on the model, could be predominantly in either the gas or particle phases. For the C_{15} and C_{17} internal alkenes, differences in calculated composition due to the treatment of dihydroxycarbonyls were small. Calculated average yields of individual products in SOA were 0.240 (DHC-gpp) and 0.265 (DHC-nv) for dihydroxycarbonyls, 0.124 for β-hydroxynitrates, 0.006 for dihydroxynitrates, and 0.021 for 1,4-hydroxynitrates. The average total SOA yields of 0.390 (DHC-gpp) and 0.418 (DHC-nv) agree very well with the measured value of 0.405 for C_{17}. As the carbon number decreased from C_{15} to C_{14}, SOA composition changed as it did for reactions of 1-alkenes, but with greater loss of compounds to the gas phase because of their higher vapor pressures.

SOA yields calculated without and with upper limit estimates for the contributions from secondary reaction products are compared with measured values over the entire carbon number range in Fig. 6A and B, respectively, and are also given in Tables S2–S4. Results shown in Fig. 6A indicate that for reactions of 1-alkenes the DHC-nv and DHC-gpp models without contributions from secondary reaction products work very well down to about C_{12} and C_{13}, respectively. Below these carbon numbers, the DHC-nv model over-predicts SOA yields by an amount that increases with decreasing carbon number, whereas the DHC-gpp model

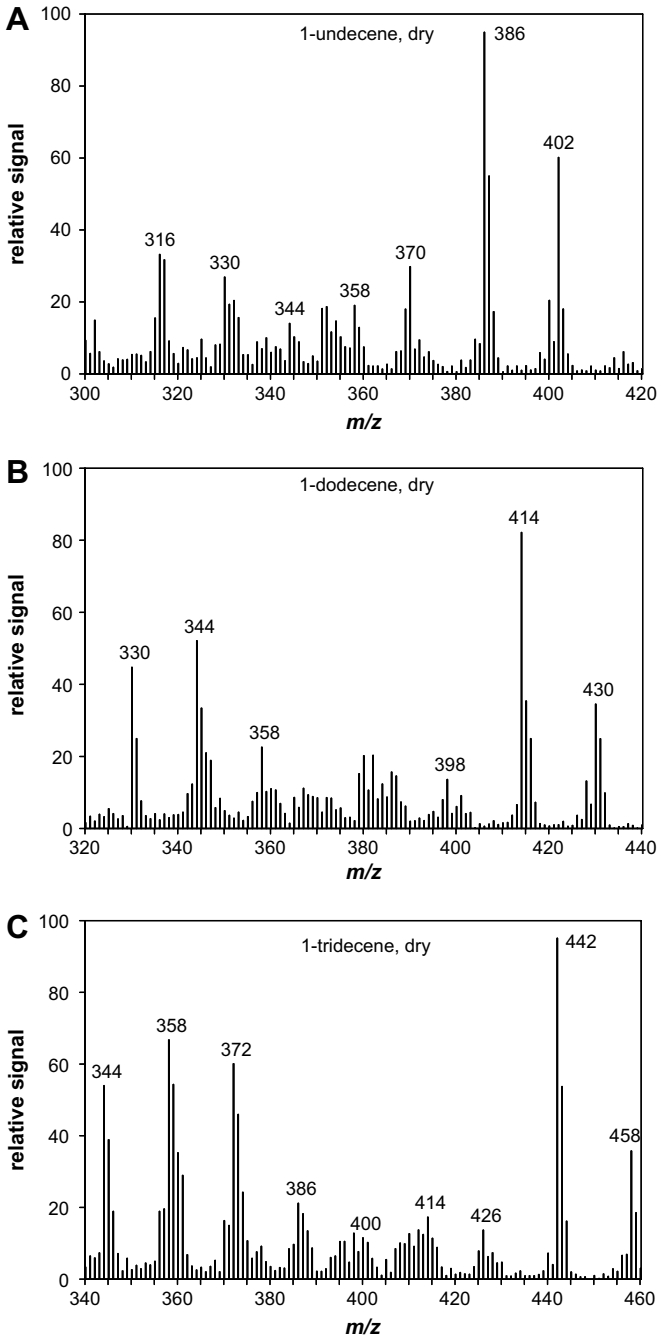

Fig. 4. Real-time mass spectra characteristic of dimers in SOA formed from the OH radical-initiated reactions of (A) 1-undecene, (B) 1-dodecene, and (C) 1-tridecene in dry air in the presence of NO_x.

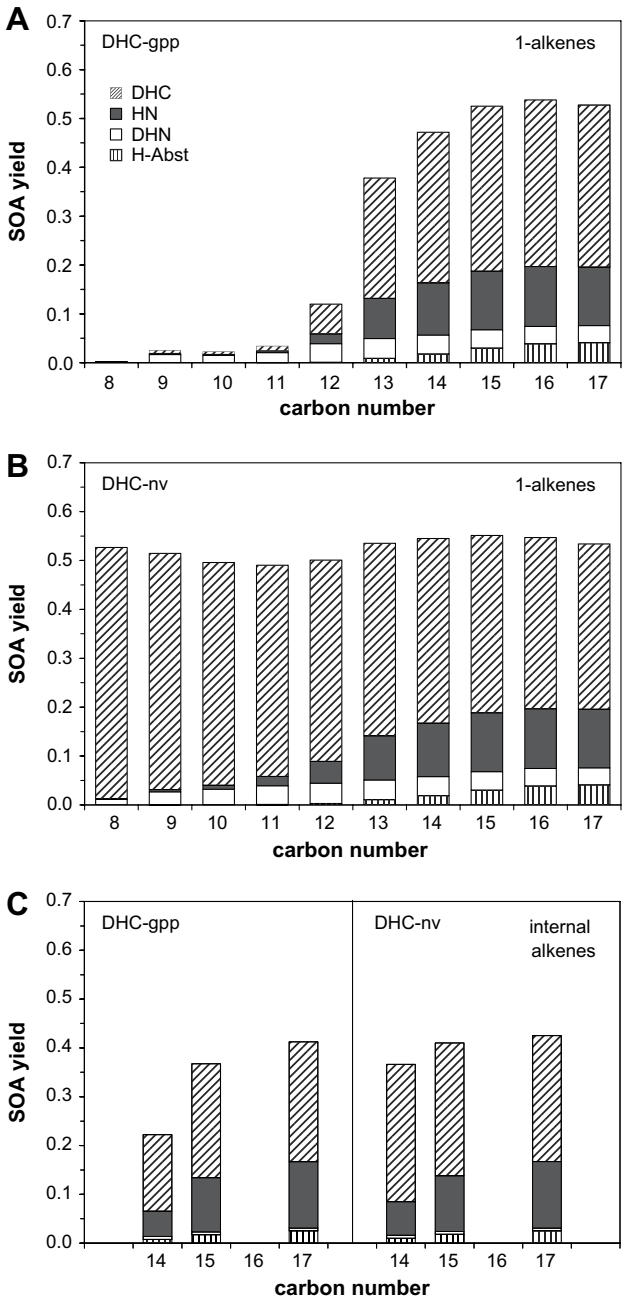

Fig. 5. Calculated yields of SOA products formed from OH radical-initiated reactions of 1-alkenes and internal alkenes in dry air in the presence of NO_x. Figures show results for dihydroxycarbonyls (DHC), β-hydroxynitrates (HN), and dihydroxynitrates (DHN) formed by OH radical addition pathways, and 1,4-hydroxynitrates formed by the H-atom abstraction (HAA) pathway. The models assumed that secondary reaction products did not contribute to SOA mass and that dihydroxycarbonyls were either (gpp) in gas-particle partitioning equilibrium or (nv) entirely in the particle phase as non-volatile cyclic hemiacetals, dihydrofurans, or dimers.

under-predicts SOA yields by an amount that decreases with decreasing carbon number. Results shown in Fig. 6A also indicate that for internal alkenes the DHC-nv and DHC-gpp models both work very well for C_{17} (and presumably at higher carbon numbers), but that for smaller carbon numbers they significantly over-predict SOA yields. This is due primarily to excess contributions from dihydroxycarbonyls, which in Fig. 2A are shown to comprise only a small fraction of the SOA mass for the 7-tetradecene reaction. A plausible explanation for this excess is that the vapor pressures used in the model for dihydroxycarbonyls formed from reactions of internal alkenes are too low by a factor of ~3, which is equivalent to a decrease of ~1 carbon number. If the vapor pressures used in the DHC-gpp model were increased by this amount, then the model curve shown in Fig. 6A would be shifted to the right by ~1 carbon number, and the agreement with measured yields would be quite good.

As expected, and as is shown in Fig. 6B, including secondary reaction products in the models increases the calculated SOA yields. Above C_{13}, the DHC-gpp and DHC-nv models both over-predict SOA yields. Below C_{13}, the DHC-nv model over-predictions are larger and the DHC-gpp model under-predictions are smaller. The best

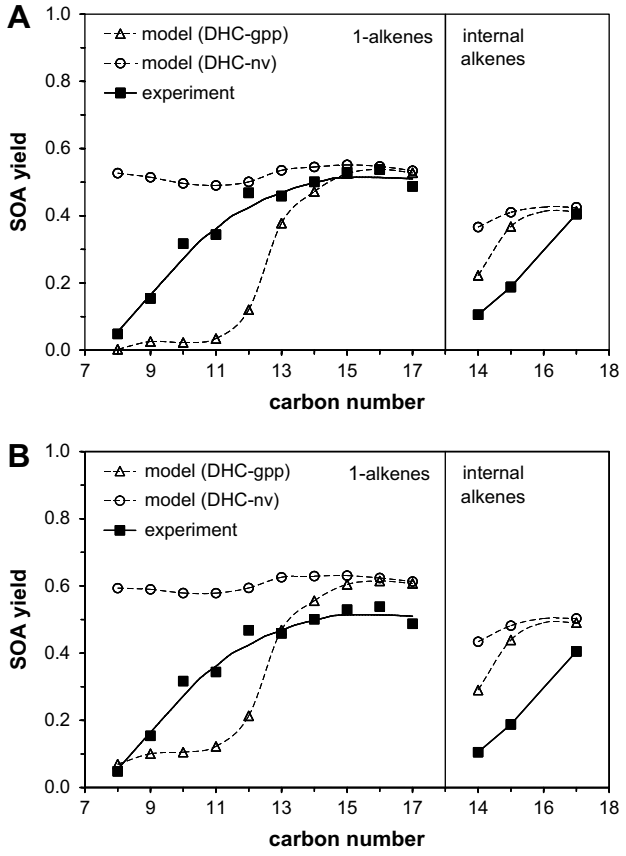

Fig. 6. Calculated and measured yields of SOA formed from OH radical-initiated reactions of 1-alkenes and internal alkenes in dry air in the presence of NO_x. The models assumed that secondary reaction products (A) did not or (B) did contribute to SOA mass and that dihydroxycarbonyls were either (gpp) in gas-particle partitioning equilibrium or (nv) entirely in the particle phase as non-volatile cyclic hemiacetals, dihydrofurans, or dimers.

region to compare these models is probably above C_{13}, since all the products are entirely in the particle phase and uncertainties due to gas–particle partitioning are therefore minimized. Results for that region suggest that secondary reaction products do not contribute significantly to SOA mass, since adding them to the model worsens the agreement between calculated and measured SOA yields.

The observation that SOA yields measured for the reactions of 1-alkenes $< C_{13}$ are between those calculated using the DHC-gpp and DHC-nv models indicates that the formation of cyclic hemiacetals, dihydrofurans, and dimers from dihydroxcarbonyls is reversible. Mass spectra show peaks due to cyclic hemiacetals, dihydrofurans, and dimers at least as small as C_9, indicating that these reactions occur for the smallest compounds studied. If the reactions were irreversible, they should lead to complete gas-to-particle partitioning of dihydroxycarbonyls and therefore SOA yields similar to those calculated using the DHC-nv model. Conversely, reversible reactions should lead to some fraction of dihydroxycarbonyls existing in the gas phase in equilibrium with the non-volatile products, and SOA yields between those calculated using the two models, as observed here. These reversible reactions cannot be incorporated into the model is a rigorous way, since there are insufficient data to constrain the particle-phase equilibria between dihydroxycarbonyls and their various reaction products. Nonetheless, if, for example, one assumes that particle-phase reactions of dihydroxycarbonyls form only dimers, then this reaction can be added to the model and the equilibrium constant, K ($m^3\ \mu g^{-1}$) = $[\text{dimer}]_p/[\text{dihydroxycarbonyl}]_p^2$, can be estimated by fitting to measured SOA yields. When this was done, a value of ~5 gave a good fit (not shown). While this is not a chemically meaningful quantity, such an approach might be sufficiently accurate for some modeling purposes.

5. Conclusions

The very good agreement between calculated and measured SOA yields for reactions of large alkenes in which gas-to-particle partitioning of dihydroxycarbonyl, β-hydroxynitrate, dihydroxynitrate, and 1,4-hydroxynitrate products is essentially complete, indicates that the chemical mechanism developed here using measured product yields and structure–reactivity methods provides an accurate representation of the gas-phase chemistry. The model should therefore be useful in this partitioning regime. The divergence between model predictions (whether assuming gas–particle partitioning equilibrium or complete gas-to-particle partitioning of dihydroxycarbonyls) and measured SOA yields for smaller alkenes is problematic, however, and clearly demonstrates the challenges to be faced in incorporating particle-phase chemistry into this and other SOA models. Fortunately, for this system the gas-phase reaction products are sufficiently well known and few in number that the particle-phase reactants and products can be identified. In particular, dihydroxycarbonyls are shown to undergo a number of reversible, particle-phase reactions to form lower volatility products. It appears that those containing a 1,4-hydroxyketone unit form cyclic hemiacetals and dihydrofurans, whereas those containing a β-hydroxyaldehyde unit form hemiacetal dimers. Previous studies of similar OH radical-initiated reactions of alkanes (Lim and Ziemann, 2005) and of reactions of alkenes with NO_3 radicals (Gong et al., 2005) have also observed the formation of cyclic hemiacetals, while studies of alkene ozonolysis have observed that hydroperoxides can undergo intramolecular or intermolecular reactions with aldehydes to form cyclic (Ziemann, 2003) and linear peroxyhemiacetals (Tobias and Ziemann, 2000).

Accurate modeling of even the simple set of particle-phase reactions identified here will require substantially more information on kinetics and thermodynamics as well as the effects of environmental variables, such as relative humidity and particle acidity. For example, it was observed (though not shown) here that SOA formation was insensitive to changes in relative humidity, but that adding ammonia reduced the formation of cyclic hemiacetals, dihydrofurans, and dimers, apparently by neutralizing nitric acid (formed by the OH + NO_2 reaction) that catalyzes the particle-phase reactions. Although acquiring such detailed information will be a challenge, it may be difficult to develop SOA models that can be applied to the laboratory or atmosphere with confidence without a much greater understanding of these types of reactions. Models recently used to simulate SOA formation from the oxidation of terpenes (Jenkin, 2004; Li et al., 2007) and aromatics (Johnson et al., 2004; Hu et al., 2007), systems known to form significant amounts of oligomers (Tolocka et al., 2004; Docherty et al., 2005; Kalberer et al., 2004), either included a set of poorly understood particle-phase reactions (for which essentially no kinetic or thermodynamic data are available), or the vapor pressures of gas-phase reaction products were reduced by 1–2 orders of magnitude below their calculated values in order to mimic the effects of particle-phase reactions on volatility.

Acknowledgments

This material is based on work supported by the National Science Foundation under Grants ATM-0328718 and ATM-0650061. Any opinions, findings, and conclusions or recommendations expressed in this material are those of the author and do not

necessarily reflect the views of the National Science Foundation (NSF). We also thank Roger Atkinson for providing results prior to publication and for helpful discussions.

Appendix. Supplementary data

Supplementary data associated with this article can be found, in the online version, at doi:10.1016/j.atmosenv.2008.12.004.

References

Altieri, K.E., Carlton, A.G., Lim, H.-J., Turpin, B.J., Seitzinger, S.P., 2006. Evidence for oligomer formation in clouds: reactions of isoprene oxidation products. Environmental Science & Technology 40, 4956–4960.

Aschmann, S.M., Atkinson, R., 2008. Rate constants for the gas-phase reactions of OH radicals with E-7-tetradecene, 2-methyl-1-tridecene, and the C_7–C_{14} 1-alkenes at 295 ± 1 K. Physical Chemistry Chemical Physics 10, 4159–4164.

Aschmann, S.M., Atkinson, R. Products and mechanism of the OH radical-initiated reactions of 1-octene and 7-tetradecene in the presence of NO. Environmental Science & Technology, in preparation.

Atkinson, R., 2007. Rate constants for the atmospheric reactions of alkoxy radicals: an updated estimation method. Atmospheric Environment 41, 8468–8485.

Atkinson, R., Arey, J., 2003. Gas-phase tropospheric chemistry of biogenic volatile organic compounds: a review. Atmospheric Environment 37 (Suppl. 2), S197–S219.

Atkinson, R., Carter, W.P.L., Winer, A.M., Pitts Jr., J.N., 1981. An experimental protocol for the determination of OH radical rate constants with organics using methyl nitrite photolysis as an OH radical source. Journal of the Air Pollution Control Association 31, 1090–1092.

Chattopadhyay, S., Ziemann, P.J., 2005. Vapor pressures of substituted and unsubstituted monocarboxylic and dicarboxylic acids measured using an improved thermal desorption particle beam mass spectrometry method. Aerosol Science and Technology 39, 1085–1100.

Colville, C.J., Griffin, R.J., 2004. The roles of individual oxidants in secondary organic aerosol formation from Δ^3-carene: 2. Soa formation and oxidant contribution. Atmospheric Environment 38, 4013–4023.

Crable, G.F., Coggeshall, N.D., 1958. Application of total ionization principles to mass spectrometric analysis. Analytical Chemistry 30, 310–313.

de Gouw, J.A., Middlebrook, A.M., Warneke, C., Goldan, P.D., Kuster, W.C., Roberts, J.M., Fehsenfeld, F.C., Worsnop, D.R., Canagaratna, M.R., Pszenny, A.A.P., Keene, W.C., Marchewka, M., Bertman, S.B., Bates, T.S., 2005. Budget of organic carbon in a polluted atmosphere: results from the New England Air Quality Study in 2002. Journal of Geophysical Research 110, D16305. doi:10.1029/2004JD005623.

Docherty, K.S., Wu, W., Lim, Y.B., Ziemann, P.J., 2005. Contributions of organic peroxides to secondary aerosol formed from reactions of monoterpenes with O_3. Environmental Science & Technology 39, 4049–4059.

Docherty, K.S., Ziemann, P.J., 2006. Reaction of oleic acid particles with NO_3 radicals: products, mechanism, and implications for radical-initiated organic aerosol oxidation. Journal of Physical Chemistry A 110, 3567–3577.

Donahue, N.M., Robinson, A.L., Stanier, C.O., Pandis, S.N., 2006. Coupled partitioning, dilution, and chemical aging of semivolatile organics. Environmental Science & Technology 40, 2635–2643.

Gong, H., Matsunaga, A., Ziemann, P.J., 2005. Products and mechanism of secondary organic aerosol formation from reactions of linear alkenes with NO_3 radicals. Journal of Physical Chemistry A 109, 4312–4324.

Heald, C.L., Jacob, D.L., Park, R.J., Russell, L.M., Huebert, B.J., Seinfeld, J.H., Liao, H., Weber, R.J., 2005. A large organic aerosol source in the free troposphere missing from current models. Geophysical Research Letters 32, L18809. doi:10.1029/2005GL023831.

Holt, T., Atkinson, R., Arey, J., 2005. Effect of water vapor concentration on the conversion of a series of 1,4-hydroxycabonyls to dihydrofurans. Journal of Photochemistry and Photobiology A – Chemistry 176, 231–237.

Hu, D., Tolocka, M., Li, Q., Kamens, R.M., 2007. A kinetic mechanism for predicting secondary organic aerosol formation from toluene oxidation in the presence of NO_x and natural sunlight. Atmospheric Environment 41, 6478–6496.

Jenkin, M.E., 2004. Modeling the formation and composition of secondary organic aerosol from α- and β-pinene ozonolysis using MCM v3. Atmospheric Chemistry and Physics 4, 1741–1757.

Johnson, D., Jenkin, M.E., Wirtz, K., Martin-Reviejo, M., 2004. Simulating the formation of secondary organic aerosol from the photooxidation of toluene. Environmental Chemistry 4, 150–165.

Johnson, D., Utembe, S.R., Jenkin, M.E., 2006. Simulating the detailed chemical composition of secondary organic aerosol formed on a regional scale during the TORCH 2003 campaign in the southern UK. Atmospheric Chemistry and Physics 6, 419–431.

Kalberer, M., Paulsen, D., Sax, M., Steinbacher, M., Dommen, J., Prevot, A.S.H., Fisseha, R., Weingartner, E., Frankevich, V., Zenobi, R., Baltensperger, U., 2004. Identification of polymers as major components of atmospheric organic aerosols. Science 303, 1659–1662.

Kanakidou, M., et al., 2005. Organic aerosol and global climate modelling: a review. Atmospheric Chemistry and Physics 5, 1053–1123.

Kern, W., Spiteller, G., 1996. Synthesis and properties of naturally occurring α-hydroxyaldehydes. Tetrahedron 12, 4347–4362.

Kroll, J.H., Seinfeld, J.H., 2008. Chemistry of secondary organic aerosol: formation and evolution of low-volatility organics in the atmosphere. Atmospheric Environment 42, 3593–3624.

Kroll, J.H., Chan, A.W.H., Ng, N.L., Flagan, R.C., Seinfeld, J.H., 2007. Reactions of semivolatile organics and their effects on secondary organic aerosol formation. Environmental Science & Technology 41, 3545–3550.

Kwok, E.S.C., Atkinson, R.J., 1995. Estimation of hydroxyl radical reaction rate constants for gas-phase organic compounds using a structure–reactivity relationship: an update. Atmospheric Environment 29, 1685–1695.

Kwok, E.S.C., Atkinson, R., Arey, J., 1996. Isomerization of β-hydroxyalkoxy radicals formed from the OH radical-initiated reaction of C_4–C_8 1-alkenes. Environmental Science & Technology 30, 1048–1052.

Li, Q., Hu, D., Leungsakul, S., Kamens, R.M., 2007. Large outdoor chamber experiments and computer simulations: (I) secondary organic aerosol formation from the oxidation of a mixture of d-limonene and α-pinene. Atmospheric Environment 41, 9341–9352.

Lim, Y.B., Ziemann, P.J., 2005. Products and mechanism of secondary organic aerosol formation from reactions of *n*-alkanes with OH radicals in the presence of NO_x. Environmental Science & Technology 39, 9229–9236.

Martin, P., Tuazon, E.C., Aschmann, S.M., Arey, J., Atkinson, R., 2002. Formation and atmospheric reactions of 4,5-dihydro-2-methylfuran. Journal of Physical Chemistry A 106, 11492–11501.

Matsunaga, A., Ziemann, P.J. Yields of β-hydroxynitrates and dihydroxynitrates in aerosol formed from the OH radical-initiated reactions of linear alkenes in the presence of NO_x. Journal of Physical Chemistry A, in press.

Nishino, N., Arey, J., Atkinson, R. Rate constants for the gas-phase reactions of OH radicals with a series of C_6–C_{14} alkenes at 299 ± 2 K. Journal of Physical Chemistry A, in press.

Odum, J.R., Hoffmann, T., Bowman, F., Collins, D., Flagan, R.C., Seinfeld, J.H., 1996. Gas/particle partitioning and secondary organic aerosol yields. Environmental Science & Technology 30, 2580–2585.

Pankow, J.F., 1994. An absorption model of the gas/aerosol partitioning involved in the formation of secondary organic aerosol. Atmospheric Environment 28, 189–193.

Presto, A.A., Donahue, N.M., 2006. Investigation of α-pinene + ozone secondary organic aerosol formation at low total aerosol mass. Environmental Science & Technology 40, 3536–3543.

Reisen, F., Ashmann, S.M., Atkinson, R., Arey, J., 2005. 1,4-Hydroxycarbonyl products of the OH radical initiated reactions of C5–C8 alkanes in the presence of NO. Environmental Science & Technology 39, 4447–4453.

Robinson, A.L., Donahue, N.M., Shrivastava, M.K., Weitkamp, E.A., Sage, A.M., Grieshop, A.P., Lane, T.E., Pierce, J.R., Pandis, S.N., 2007. Rethinking organic aerosols: semivolatile emissions and photochemical aging. Science 315, 1259–1262.

Seinfeld, J.H., Pandis, S.N., 1998. Atmospheric Chemistry and Physics. John Wiley & Sons, New York.

Seinfeld, J.H., Erdakos, G.B., Asher, W.E., Pankow, J.F., 2001. Modeling the formation of secondary organic aerosol (SOA). 2. The predicted effects of relative humidity on aerosol formation in the α-pinene-, β-pinene-, sabinene-, Δ^3-carene-, and cyclohexene–ozone systems. Environmental Science & Technology 35, 1806–1817.

Taylor, W.D., Allston, T.D., Moscato, M.J., Fazekas, G.B., Kozlowski, R., Takacs, G.A., 1980. Atmospheric photodissociation lifetimes for nitromethane, methyl nitrite, and methyl nitrate. International Journal of Chemical Kinetics 12, 231–240.

Tobias, H.J., Ziemann, P.J., 1999. Compound identification in organic aerosols using temperature-programmed thermal desorption particle beam mass spectrometry. Analytical Chemistry 71, 3428–3435.

Tobias, H.J., Ziemann, P.J., 2000. Thermal desorption mass spectrometric analysis of organic aerosol formed from reactions of 1-tetradecene and O_3 in the presence of alcohols and carboxylic acids. Environmental Science & Technology 34, 2105–2115.

Tobias, H.J., Kooiman, P.M., Docherty, K.S., Ziemann, P.J., 2000. Real-time chemical analysis of organic aerosols using a thermal desorption particle beam mass spectrometer. Aerosol Science and Technology 33, 170–190.

Tolocka, M.P., Jang, M., Ginter, J., Cox, F., Kamens, R., Johnston, M., 2004. Formation of oligomers in secondary organic aerosol. Environmental Science & Technology 38, 1428–1434.

Volkamer, R., Jimenez, J.L., San Martini, F., Dzepina, K., Zhang, Q., Salacedo, D., Molina, L.T., Worsnop, D.R., Molina, M.J., 2006. Secondary organic aerosol formation from anthropogenic air pollution: rapid and higher than expected. Geophysical Research Letters 33, L17811. doi:10.1029/2006GL026899.

Wang, S.C., Flagan, R.C., 1990. Scanning electrical mobility spectrometer. Aerosol Science and Technology 13, 230–240.

Weber, R.J., Sullivan, A.P., Peltier, R.E., Russell, A., Yan, B., Zheng, M., de Gouw, J., Warneke, C., Brock, C., Holloway, J.S., Atlas, E.L., Edgerton, E., 2007. A study of secondary organic aerosol formation in the anthropogenic-influenced southeastern United States. Journal of Geophysical Research 112, D13302. doi:10.1029/2007JD008408.

Ziemann, P.J., 2003. Formation of alkoxyhydroperoxy aldehydes and cyclic peroxyhemiacetals from reactions of cyclic alkenes with O_3 in the presence of alcohols. Journal of Physical Chemistry A 107, 2048–2060.